LIP-STUDENTS-25-29

Energy Calibration of SND@LHC

João Galhardo[1,a]

[1] *Instituto Superior Técnico, Lisboa, Portugal*

Project supervisors: Nuno Leonardo, Cristóvão Vilela

December 2, 2025

Abstract. The purpose of this work is to study the impact of the saturation effect of scintillator bars on existing simulation software and to evaluate the results through comparison with real data, determining whether or not it has a positive impact on how accurate the data provided by the simulation software is.

Keywords: SND@LHC, Calibration, Scintillator

1 The SND@LHC

The SND@LHC is a dedicated neutrino experiment, currently operating at the LHC [2]. It is the most recent LHC experiment, having been deployed in 2022, at the start of LHC Run 3.

It is a novel detector, built for the detection of high-energy neutrinos [1] and, much like any new detector, it needs to be calibrated. For purpose of calibrating the energy response of the detector, and the development of the associated methods, another detector, the *test detector*, was built as an approximate replica of SND@LHC (which itself is installed and operating at the LHC) [3].

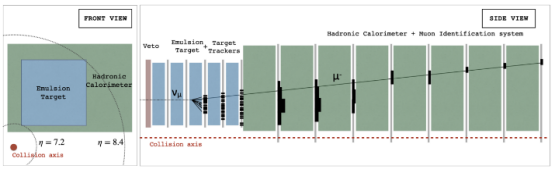

Figure 1. Simplified schematics of the SND@LHC detector [2].

The SND@LHC detector has three main components, of which only two exist in the test detector. Firstly, we have the veto. It is the front part of SND@LHC and allows for the detection of incoming charged particles, like muons. It is formed of two scintillator planes, and is not replicated on the test detector.

Following the veto, we have the target. In SND@LHC, it is composed of tungsten and emulsion detector plates, interpolated with planes made of scintillating fibers. For the test detector, the target is composed only of iron planes and scintillator fiber planes. It tracks the spatial and time trajectories of passing particles.

Lastly, there is the hadronic calorimeter and the muon system. The calorimeter is made of iron plates and planes of scintillator bars, both in the SND@LHC and in the test detector. The calorimeter is complemented with a Muon Identification system, not present in the test detector, that serves to detect muons leaving the detector.

To understand the purpose of the calorimeter, it is necessary to know what happens when the high-energy neutrinos interact in the target. Simply put, when the neutrino interacts with a nucleus in the tungsten planes, the high energy of the interaction breaks the nucleus and creates a shower of particles that will propagate through the detector. The calibration of the detector revolves around determining the energy of this shower, and the calorimeter is the main tool used for this purpose.

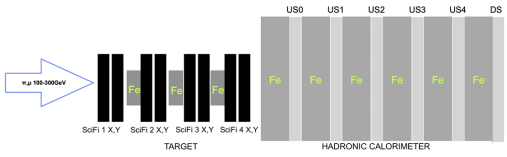

Figure 2. Schematics of *test detector* used in calibration [3].

1.1 The simulation and Birk's Law

Part of the calibration studies uses software that simulates the test detector. The calibration process utilizes charged particles with specific energies that cause a hadronic shower; in the case of the test detector, the particles used are pions. Up until now, the simulated data provided by the software has not been accurate when compared to real data, indicating a need to further improve the simulation software. In this article, we explore the saturation effects on the scintillator bars of the calorimeter by introducing a saturation effect in the treatment of the simulated data.

When a particle travels through a scintillator bar it deposits energy per distance traveled ($\frac{dE}{dx}$). This energy is converted into a luminous signal in the scintillator, which is then absorbed by a photomultiplier and converted into an electric signal (QDC). The saturation effect appears in the relation between the luminous signal and the deposited energy. This relation can be described through Birk's Law:

$$QDC \propto \frac{dL}{dx} = \frac{S \times \frac{dE}{dx}}{1 + kB \times \frac{dE}{dx}} . \tag{1}$$

It reflects the relation between light yield and energy, both per unit of distance traveled by the particle, $\frac{dL}{dx}$ and energy loss $\frac{dE}{dx}$. The remaining terms are constants intrinsic to the detector: S is the detector efficiency, which we consider to be 1, and kB is Birk's coefficient.

[a] e-mail: joao.m.c.galhardo@tecnico.ulisboa.pt

The result of applying this expression is that, although the scintillating behavior for particles with lower $\frac{dE}{dx}$ remains linear, when this value increases the light yield becomes less than what it would be if the behavior were linear.

2 Simulation data

To introduce the saturation effect we first apply Birk's Law to the simulated data on the calorimeter. The process is simplified as we consider that on average a particle travels the depth of a scintillator bar, which is 1 cm, and since the simulation records all the energy deposits throughout the calorimeter we can approximate Birk's Law substituting $dx = 1$ cm on 1. Then to get the actual energy released on the scintillator we sum all contributions,

$$\Sigma dL = \Sigma \frac{S \times dE}{1 + kB \times dE} \,. \tag{2}$$

We can then compare the results to the previous method of handling data, where we assumed that the energy released on the scintillator was the same as the deposited energy. The data used here corresponds to pions with an energy of 180 GeV.

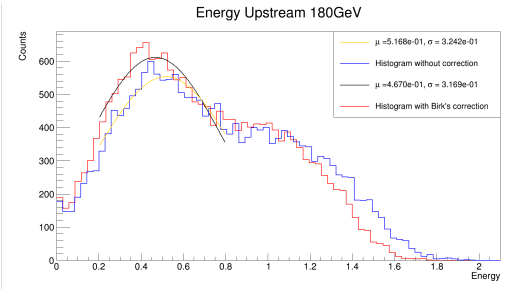

Figure 3. Data distributions, corrected and non-corrected.

For further analysis, the peak of the distributions has been calculated through a localized fit, yielding values of $\mu_B = 0.52$ for the corrected data, and of $\mu = 0.47$ for the non-corrected data. We note that there is no dimension for the energy as a result of no energy calibrations having been made.

Analyzing the distributions, we can see that, with the application of Birk's law, the data retreats towards the origin. Furthermore, as we will see later, this effect is stronger for higher energy values.

2.1 Data Analysis

The method used to analyze the data is crude and is a simple way for comparing the raw data with the corrected data. The first step consists of finding the normalized cumulative distribution of the previous histograms from the peak of the distribution onward. Since these peaks have already been determined, we can proceed to getting the cumulative distributions, as shown in Fig. 4.

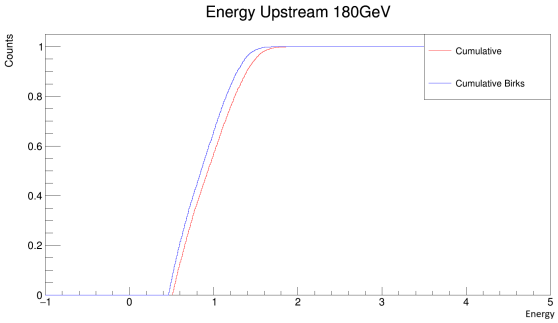

Figure 4. Cumulative distributions obtained from Fig. 3.

This step allows us to see the difference brought about by applying Birk's Law a bit more clearly.

We can now compare the simulated data to the real data. This real data does not represent the individual depositions of energy, as in the simulation, but the sum of all the signals emitted by the calorimeter. While a direct comparison is not feasible, the response of the detector provided by the simulation still needs to be improved, so this will act as a first step towards such improvement. We apply the same process of finding the peak of the distribution of the real data from the test detector, and from there we get the cumulative distribution. From all three cumulative distributions, we register four points at the same heights, and this allows us to create two sets of points comparing the *QDC* values of the simulated data distributions with the real data distribution, as shown in Fig. 5.

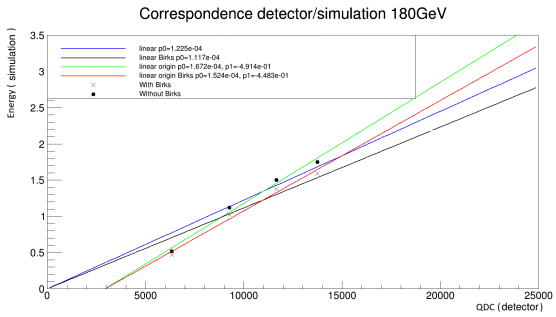

Figure 5. Real data *vs* Simulated data.

We apply two linear fits to both sets of points, one with free parameters and the other passing through the origin. Here, although we are not comparing both simulated sets of data directly, it becomes clearer how the saturation effect is more noticeable for higher energies.

From Fig. 5, we can obtain a value that allows the scaling of the real data to the simulated data, and the comparison of the original histograms, shown in Fig. 6.

One of the main problems of the simulated data was its abnormal behavior at higher energies, where the distributions acquired a tail that did not fit real data. In Fig. 6, we can see that this problematic characteristic is corrected with Birk's law as the tail of the distribution retreats fitting in the real data. Another problem associated with the op-

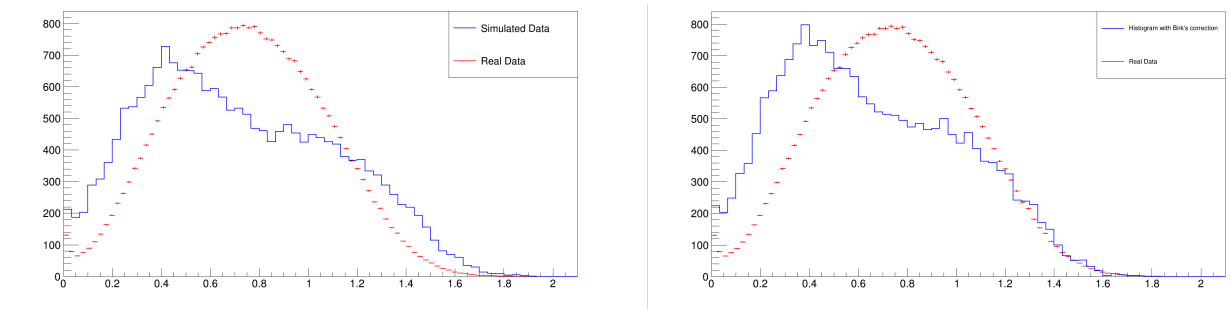

Figure 6. (Left) Raw and simulated data; (Right) Data and simulation, with Birk's law correction.

posite side of the distribution remains almost unaltered, as the effect of Birk's Law is weaker towards lower energies.

3 Conclusion

We conclude that introducing Birk's Law to account for saturation losses on the hadronic calorimeter results in an improved description, eliminating one of the main discrepancies observed between the simulation and real data. A possible way to improve on these results could be by considering additional saturation effects.

References

[1] SND@LHC. In: *PRL* 131 (2023), p. 031802. DOI: 10.1103/PhysRevLett.131.031802.

[2] SND@LHC. "SND@LHC: the scattering and neutrino detector at the LHC". In: *JINST* 19 (2024), P05067. DOI: 10.1088/1748-0221/19/05/P05067.

[3] SND@LHC. "Studies of hadronic showers in SND@LHC". In: *JINST* 20 (2025), P10039. DOI: 10.1088/1748-0221/20/10/P10039.